Spectrochimica Acta Part A: Molecular and Biomolecular Spectroscopy 116 (2013) 622–634

Contents lists available at ScienceDirect

Spectrochimica Acta Part A: Molecular and Biomolecular Spectroscopy

journal homepage: www.elsevier.com/locate/saa

FT-IR and FT-Raman, NMR and UV spectroscopic investigation and hybrid computational (HF and DFT) analysis on the molecular structure of mesitylene

E. Kose [a,*], A. Atac [a], M. Karabacak [b], P.B. Nagabalasubramanian [c], A.M. Asiri [d,e], S. Periandy [f]

[a] Department of Physics, Celal Bayar University, Manisa, Turkey
[b] Department of Mechatronics Engineering, H.F.T. Technology Faculty, Celal Bayar University, Manisa, Turkey
[c] Department of Physics, Arignar Anna Govt. Arts College, Karaikal, Puducherry State, India
[d] Center of Excellence for Advanced Materials Research (CEAMR), King Abdulaziz University, Jeddah, Saudi Arabia
[e] Department of Chemistry, Faculty of Science, King Abdulaziz University, Jeddah, Saudi Arabia
[f] Department of Physics, Tagore Arts College, Puducherry, India

HIGHLIGHTS

- Molecular structure of mesitylene was investigated.
- The FT-IR and Raman spectra of mesitylene were compared with calculated spectra.
- The vibrational frequencies were calculated by DFT method and discussed.
- The complete assignments are performed on the basis of the total energy distribution (TED).
- NMR and UV spectra were compared with calculated ones.

GRAPHICAL ABSTRACT

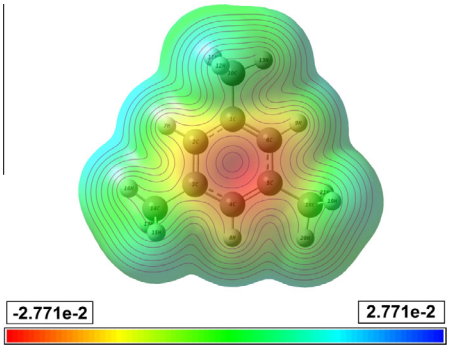

ARTICLE INFO

Article history:
Received 17 April 2013
Received in revised form 8 July 2013
Accepted 25 July 2013
Available online 6 August 2013

Keywords:
Mesitylene
DFT and HF
FT-IR
Raman
UV
NMR
HOMO–LUMO

ABSTRACT

The spectroscopic properties of mesitylene were investigated by FT-IR, FT-Raman, UV, ^{1}H and ^{13}C NMR techniques. The geometrical parameters and energies have been obtained from density functional theory (DFT) B3LYP method and Hartree–Fock (HF) method with 6-311++G(d,p) and 6-311G(d,p) basis sets calculations. The geometry of the molecule was fully optimized, vibrational spectra were calculated and fundamental vibrations were assigned on the basis of the total energy distribution (TED) of the vibrational modes, calculated with scaled quantum mechanics (SQM) method and PQS program. Total and partial density of state (TDOS and PDOS) and also overlap population density of state (OPDOS) diagrams analysis were presented. ^{13}C and ^{1}H NMR chemical shifts were calculated by using the gauge-invariant atomic orbital (GIAO) method. The electronic properties, such as excitation energies, oscillator strength, wavelengths, HOMO and LUMO energies, were performed by time-dependent density functional theory (TD-DFT) results complements with the experimental findings. The results of the calculations were applied to simulate spectra of the title compound, which show excellent agreement with observed spectra. Besides, frontier molecular orbitals (FMO), molecular electrostatic potential (MEP) and thermodynamic properties were performed. Reduced density gradient (RDG) of the mesitylene was also given to investigate interactions of the molecule.

* Corresponding author. Tel.: +90 236 201 3131.
E-mail address: etemmm43@gmail.com (E. Kose).

1386-1425/$ - see front matter © 2013 Elsevier B.V. All rights reserved.
http://dx.doi.org/10.1016/j.saa.2013.07.070

Introduction

Mesitylene is the common name of 1,3,5-Trimethyl benzene (triply methylated benzene, $C_6H_3(CH_3)_3$ is a derivative of benzene with three methyl substituents symmetrically (in the C_3 symmetry positions) placed on the benzene ring and among the simplest aromatic hydrocarbon. It is the most symmetric isomer with three methyl groups and is the only methyl containing compound which can be stabilized in three different phases at the temperature. The solid mesitylene has high efficiency as a neutron moderator which makes the material a promising candidate for an improved cold neutron moderator at future spallation sources due to the rotational freedom of methyl groups and its high hydrogen density [1]. It is naturally occurring in petroleum and coal tar which is also is used as a solvent for resins, gums, nitrocellulose, in manufacturing of lacquers, paints and varnishes. It is an intermediate for the manufacture of antioxidants, as ligand in organometallic chemistry and due to its solvent properties; it is used as developer for photo patternable silicones in electronics industry. It plays an important role in the formation of tropospheric ozone. Owing to identical chemical shift environment of three aromatic hydrogen atoms of mesitylene, it is used as an internal standard in NMR samples.

The vibrational spectra of mesitylene were studied by the earlier literatures [2–8]. Lokshin et al. [9] reported and discussed the IR and Raman spectra of mesitylene. The low frequency internal vibrations of mesitylene with neutron spectroscopy were carried out with IINS spectra at 290, 100 and 18 K. The isolated molecule was interpreted with the atomic coordinates and normal modes frequencies using semi-empirical quantum chemistry method [10]. The air–liquid interface and the liquid-phase of mesitylene, benzene, toluene, and 1,3-dimethylbenzene are studied using broad bandwidth sum frequency generation spectroscopy by Hommel and Allen [11]. Reorientation of mesitylene in the neat liquid has been investigated using a combination of IR and Raman techniques [12].

The potential and structural implications with rotational tunneling of methyl groups in low temperature phases of mesitylene were carried out [13]. The calculation of the valence force constants for the non-planar vibrations of the 1,3,5 trimethyl-benzene molecule were studied in the earlier literatures [14]. Molecular deformations of halogen-mesitylene in the crystal: structure, methyl group rotational tunneling, and numerical modeling was performed by Trommsdorff et al. [15]. The distribution of mesitylene and 3,5-dimethylbenzoic acid in tissues as well as the kinetics of mesitylene excretion with blood and 3,5-dimethylbenzoic acid excretion with urine in rats after termination of single and repeated inhalation exposures to mesitylene at concentrations of 25, 100, and 250 ppm were performed [16]. The study determination of the equilibrium constants for the hydrogenation of mesitylene was reported by Egan and Buss [17]. The vibrational spectra of triiodo-mesitylene were studied with the combination of DFT calculations and experimental results [18]. The vibrational spectra of mesitylenechromium tricarbonyl and mesitylenemolybdenum tricarbonyl molecule were reported earlier [19]. Hernandez et al. were studied the phases of 1,3,5-trichloro-2,4,6-trimethylbenzene using ab initio crystal structure determination by high-resolution powder diffraction [20].

With the aid of above seen literatures, it is clear that there is no quantum mechanical study on this title molecule which has motivated to do a detailed quantum mechanical analysis for understanding the vibrational modes, chemical shifts, HOMO–LUMO, MEP, Mulliken atomic charge and thermodynamic properties, also RDG of title compound. The aim of this study is to calculate optimal molecular geometry, vibrational frequencies, and chemical shifts of mesitylene. The complete analysis was performed by combining the experimental and theoretical information using Pulay's DFT based scaled quantum chemical approach [21]. The vibrational wavenumbers, geometrical parameters, modes of vibrations, atomic charges, other thermodynamic parameters, HOMO–LUMO and UV of this molecule were investigated by using HF and B3LYP calculations with 6-311G(d,p) and 6-311++G(d,p) basis sets. Specific scale factors were employed in the predicted frequencies. The detailed interpretations of the vibrational spectra of the mesitylene have been made on the basis of the calculated TED. All results which were examined before by the experimental (IR, Raman, NMR and UV spectra) were supported by the computed results, comparing with experimental characterization data; vibrational wavenumbers, absorption wavelengths, electronic properties and chemical shifts values are in fairly good agreement with the experimental results.

Computational details

The infrared and Raman spectra of the title molecule were taken from Standard Reference Datas of National Institute of Standards and Technology, NIST [22] and Spectral Database for Organic Compounds, SDBS [23]. The ultraviolet absorption spectrum of the mesitylene was taken NIST [22]. The data of NMR also was taken from SDBS [23]. All the experimental reports of mesitylene were evaluated by comparing theoretical calculations of the mesitylene.

The molecular structure optimization and corresponding vibrational harmonic frequencies of mesitylene were calculated using ab-intio HF and DFT calculations [24] with the Becke's three-parameter hybrid functional (B3) [25] for the exchange part and the Lee–Yang–Parr (LYP) correlation function [26], for the computation of molecular structure, vibrational frequencies and energies of optimized structures by using Gaussian 09 suite of quantum chemical codes [27]. Gaussian 09 program package was used without any constraint in the geometry with split valence basis sets along with diffuse and polarization function with 6-311++G(d,p) and split valence basis sets along with polarization function with 6-311G(d,p) both HF and DFT methods.

Firstly, the title molecule was optimized, after then the optimized structural parameters were used in the vibrational frequency, isotropic chemical shift and calculations of electronic properties. The vibrational frequencies, Infrared and Raman intensities for the C_{3h} symmetry structure of the title molecule were calculated. In order to improve the calculated values in agreement with the experimental values, it is necessary to scale down the calculated harmonic frequencies. Hence, the vibrational frequencies calculated at HF level are scaled by 0.9067, and the range of wave numbers above 1700 cm^{-1} are scaled as 0.958 and below 1700 cm^{-1} scaled as 0.983 for B3LYP [28,29]. After scaled with the scaling factor, the deviation from the experiments is less than 10 cm^{-1} with a few exceptions. The TED calculations were carried out by the SQM method [30] using PQS program [31] and the fundamental vibrational modes were characterized by their TED, which showed the relative contributions of the redundant internal coordinates to each normal vibrational mode of the molecule and thus enable us numerically to describe the character of each mode.

The isotropic chemical shifts are frequently used as an aid in identification of organic compounds and accurate predictions of molecular geometries are essential for reliable studies of magnetic properties. The ^{13}C and ^{1}H NMR isotropic shielding were calculated with the GIAO method [32,33] using the optimized parameters obtained from B3LYP/6-311++G(d,p) method. The GIAO method is one of the most common approaches for calculating nuclear magnetic shielding tensors.

In order to understand the electronic properties, such as HOMO–LUMO energies, dipole moment, absorption wavelengths,

and oscillator strengths were calculated using B3LYP method of the TD-DFT [34–37] and 6-311++G(d,p) basis set, based on the optimized structure. The changes in the thermodynamic functions (the heat capacity, entropy, and enthalpy) were investigated for the different temperatures from the vibrational frequency calculations of title molecule.

Besides of these calculations, the group contributions of the molecular orbitals and to prepare TDOS (or DOS), PDOS and OPDOS spectra GaussSum 2.2 [38] was used. The contribution of the group to a molecular orbital was calculated using Mulliken population analysis. The PDOS and OPDOS spectra were created by convoluting the molecular orbital information with Gaussian curves of unit height and a FWHM (Full Width at Half Maximum) of 0.3 eV. Also The Reduced density gradient (RDG) of the title molecule were graphed by Multiwfn and plotted by VMD program [35,39].

Results and discussion

The molecule of the mesitylene has three substituents such that CH_3 groups attached to a planar benzene ring. The mesitylene consists of 21 atoms and it has 57 normal vibrational modes. On the basis of a C_{3h} symmetry, the 57 fundamental vibrations of the mesitylene can be distributed as $14E'' + 7A'' + 24E' + 12A'$. The energies of the title molecule were calculated using by HF and B3LYP calculations with 6-311G(d,p) and 6-311++G(d,p) basis sets. The relative energy of the other basis sets was as: $\Delta E = E_{\mathbf{t}} - E_{\mathbf{a}}$, the **t:** other basis sets and **a** is the lowest energy as reference point are given in Table S1. The energies and energy difference of the molecule also reported in the same table. The variation in zero-point vibrational energies (ZPVEs) seems to be significant. The ZPVE is much lower by the DFT B3LYP method than by the HF method. The biggest value of ZPVE of title molecule is 121.22076 kcal/mol obtained at HF method whereas the smallest value is 113.85491 kcal/mol obtained at B3LYP/6-311++G(d,p). The energy value is obtained DFT calculation with 6-311++G(d,p) basis set is computed more stable from 1.7557 kcal/mol to 1507.0756 kcal/mol than the other basis sets. As we can see the Table S1, imaginary frequencies of the title molecule were leaped out using by B3LYP calculations with 6-311G(d,p) basis set however were not seen by HF method with 6-311G(d,p), 6-311++G(d,p) basis sets and B3LYP method 6-311++G(d,p) basis set. Specific heat, C_v, is calculated 33.237 (cal mol^{-1} K^{-1}) for HF method for two basis sets. However this value were obtained 29.592 and 35.561 (cal mol^{-1} K^{-1}) with B3LYP method 6-311G(d,p) and 6-311++G(d,p) basis sets. The similar changes were seen entropy values. The geometric parameters (bond lengths and bond angles), vibrational frequencies, NMR shifts and UV absorption of title were molecule reported by comparing experimental results in following sections.

Geometrical structures

The crystal structure of the trichloro-mesitylene [20] structurally similar molecules with our tittle molecule were studied; however mesitylene is not available in the literature until now, therefore, the geometric parameters, bond lengths and bond angles, compared with this molecule. The atomic numbering scheme of the mesitylene is shown in Fig. 1. The optimized geometry parameters (bond lengths and bond angles) of the molecule are given in Table 1, comparing to the experimental values, in accordance with the atom numbering Fig. 1. It is seen that from Table 1, the B3LYP levels of theory is computed slightly bigger than experimental values of mesitylene. However HF method is calculated more closely than the B3LYP method. The calculations of geometric parameters were performed both 6-311G(d,p) and 6-311++G(d,p) basis sets for each method (B3LYP and HF). There is

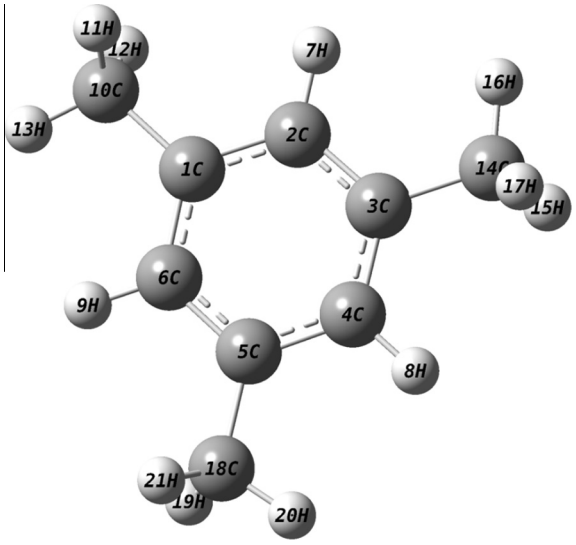

Fig. 1. The theoretical geometric structures of mesitylene.

not seen important difference between 6-311G(d,p) and 6-311++G(d,p) basis sets of the methods. The C—C bond lengths of between ring and methyl groups (CH_3) are bigger than the C—C bond of in the ring. The C—H bonds (CH_3) for the title molecule are approximately equal to for experimental values [20]. The C—H bond lengths are computed in the range 1.080–1.095 Å observed as a 0.980 Å [40] for CH_3 groups and the bond C—H are also computed between 1.070 and 1.085 Å (exp. 0.950 Å [40]) for the ring part. Also average C—H bond lengths for methyl group was computed at 1.094 and 1.085 Å B3LYP and HF method with the 6-311++G(d,p) basis set for 2,5-Lutidine [40]. The similar behaviors are valid between the C—C bond lengths and angles (ring) by using for each method. The optimized bond lengths of C—C in benzene ring were calculated between 1.379 and 1.404 Å [40]. In our present study the CC bond lengths are computed from 1.380 to 1.402 Å showing a closer agreement with the experimental data and literature [40,41]. As the seen some differences between calculated and experimental could be due to the fact that the calculations are obtained from gas phase however experimental results are taken solid phase. The ring C—C—C, bond angles observed in the range of 115.5–124.5° [20] show well correlation with the calculated values. The symmetry of the benzene ring is distorted, yielding ring angles smaller than 120° and slightly larger than 120° at the point of the substitutions (methyl groups). All calculated bond angles showed the small difference from experimental values, also this can be due to calculation belongs to vapor phase and experimental result belong to solid phase. One can quite easily see from Table 1, all the calculations of bond angles are in very consistency with the compared experimental values and similar literature [20,41–43].

Vibrational spectral analysis

The vibrational frequencies were obtained from the DFT/B3LYP and HF methods by using split valence basis sets along with diffuse and polarization function with 6-311++G(d,p) and split valence basis sets along with polarization function with 6-311G(d,p). The recorded infrared [22] and Raman [23] spectra of mesitylene and also the calculated vibrational wavenumbers (the energy of the 6-311++G(d,p) basis set are more stable than 6-311G(d,p) basis set were given due to head of the mesitylene of the most stable energy for each method) and assignments with the TED are given in Tables 2 and S2 for title molecule.

Table 1
Bond lengths (Å) and bond angles (°) for experimental and optimized of mesitylene.

Parameters	HF		B3LYP		
	6-311G(d,p)	6-311++G(d,p)	6-311G(d,p)	6-311++G(d,p)	Exp. values [a]
Bond lengths (Å)					
C_1—C_2	1.397	1.397	1.402	1.402	1.409
C_1—C_6	1.380	1.380	1.392	1.393	1.382
C_1—C_{10}	1.511	1.511	1.511	1.511	1.491
C_2—C_3	1.380	1.380	1.392	1.393	1.374
C_3—C_4	1.397	1.397	1.402	1.402	1.374
C_3—C_{14}	1.511	1.511	1.511	1.511	1.512
C_4—C_5	1.380	1.380	1.392	1.393	1.421
C_5—C_6	1.397	1.397	1.402	1.402	1.397
C_5—C_{18}	1.511	1.511	1.511	1.511	1.525
C—H_{ring} (average)	1.077	1.077	1.086	1.087	–
C—H_{methyl} (average)	1.085	1.085	1.093	1.094	1.089
Bond angles (°)					
C_2—C_1—C_6	118.7	118.7	118.5	118.5	115.7
C_2—C_1—C_{10}	120.0	120.0	120.3	120.3	121.3
C_6—C_1—C_{10}	121.3	121.3	121.2	121.2	122.9
C_1—C_2—C_3	121.3	121.3	121.5	121.5	123.5
C_2—C_3—C_4	118.7	118.7	118.5	118.5	117.8
C_2—C_3—C_{14}	121.3	121.3	121.2	121.2	121.4
C_4—C_3—C_{14}	120.0	120.0	120.3	120.3	120.7
C_3—C_4—C_5	121.3	121.3	121.5	121.5	122.8
C_3—C_4—H_8	119.2	119.2	119.2	119.2	—
C_4—C_5—C_6	118.7	118.7	118.5	118.5	115.5
C_4—C_5—C_{18}	121.3	121.3	121.2	121.2	122.9
C_6—C_5—C_{18}	120.0	120.0	120.3	120.3	121.6
C_1—C_6—C_5	121.3	121.3	121.5	121.5	124.5
C_1—C_6—H_9	119.5	119.5	119.3	119.3	—
C—C—H_{methyl} (average)	111.0	111.0	111.3	111.3	109.6
H—C—H_{methyl} (average)	107.9	107.9	107.6	107.6	107.6

[a] The X-ray data from Ref. [20].

The experimental [22,23] and calculated (both B3LYP and HF methods for two basis sets) infrared and Raman spectra were given in Fig. 2. The calculated IR and Raman spectra are shown in figure for comparative purpose, where the calculated intensity is plotted against harmonic vibrational wavenumbers.

This part of the study deals with assignment of the vibrational absorptions to make a comparison with the related molecules and also the results obtained from the theoretical calculations. There are some strong frequencies useful to characterize in the IR and Raman spectra.

C—H stretching modes

The title molecule gives rise to C—H modes such as stretching, in-plane and out-of-plane bending vibration. Aromatic compounds commonly exhibit multiple weak bands in the region 3000–3100 cm^{-1} [44] due to aromatic C—H stretching vibrations. The C—H in-plane bending frequencies appear in the range of 1000–1300 cm^{-1} and C—H out-of-plane bending vibration in the range 750–1000 cm^{-1} for aromatic compounds [45,46]. The aromatic C—H stretching bands are found to be weak, and this is due to a decrease in the dipole moment caused by reduction of negative charge on the carbon atom. The title molecule has two type CH modes; CH modes in the ring and the CH_3 modes of substituted methyl groups. As indicated by the TED, these twelve modes (ν46–57) involve ca. 95–100% contribution.

The C—H stretching modes in the ring were calculated 3013–3016 cm^{-1} and recorded at 3007 and 3009 cm^{-1} in infrared and Raman spectra [22]. In the present study, the three adjacent hydrogen atoms left around the ring the title molecule give rise three CH stretching modes (modes 55–57), which corresponds to stretching modes of C2–H7, C4–H8, C6–H9 units. In the ring, the symmetric stretch is at slightly higher wavenumber than the asymmetric stretch. In this study, the C—H symmetric stretching mode is calculated at 3016 cm^{-1} and recorded strong mode at 3017 cm^{-1} in infrared [9]. The asymmetric stretching mode is obtained at 3009 cm^{-1} [22] and calculated at 3013 cm^{-1}. These modes also are pure and show characteristic properties for the molecule. The calculated CH stretch modes scaled down showing good correlation with the experimentally observed vibrations. The theoretical vibrational spectrum (Fig. 2) and calculated wavenumbers (Tables 2 and S2) of the molecule show very good correlation with their experimental results. The C—H (methyl group) stretching vibrations are lower than the ring C—H (ring) stretching vibrations.

The C—H bending vibrations are predicted in the region ca. 900–1650 cm^{-1} (in-plane) and ca. 170–222 and ca. 600–900 cm^{-1} (out-of plane) (Tables 2 and S2) and observed values are coinciding very well with these frequencies. As one can see tables the CH in plane bending modes are range after 900 cm^{-1} for example; 927, 1167, 1274, 1299, 1323,, 1433, 1461, 1470, 1487 and 1613 cm^{-1} with the B3LYP method and 909, 1153, 1159, 1299, 1425, 1458, 1476, and 1619 cm^{-1} with the HF method. The experimental [22] results were recorded at 927, 1065, and 1608 cm^{-1} in FT-IR and 1070, 1302, and 1610 cm^{-1} in FT-Raman spectra. Also the TED were showed that the mode 28 and 29 have been biggest contribution (nearly%50). However the in-plane bending vibrations are contaminated other modes. Some modes of CH_3 in plane modes are assigned as the rocking and twisting. These modes are also given next part in their named.

The C—H out plane bending modes are defined the lower frequencies than the in plane modes. The out of plane C—H modes are showed nearly pure modes according to TED and assignment of Gaussview program. These modes are computed at 169, 217(double), 521 (double), 695, 838, 879 cm^{-1} (double) using by B3LYP method and also at 171, 221(double), 526 (double), 693, 850, 898 cm^{-1} (double) using by HF method, showed a good agreement with the experimental data. The recorded results [9] were at 179, 836 and 881 cm^{-1} in FT-IR and 183, 231, 835 and 881 cm^{-1} in FT-Raman spectra. The TED contributions of modes are also highly

Table 2
Comparison of the calculated harmonic frequencies and experimental (FT-IR and FT-Raman) wavenumbers (cm^{-1}) using by B3LYP method 6-311++G(d,p) basis set of mesitylene.

Modes	Sym.	B3LYP/6-311++G(d,p)		Experimental[b]		Experimental[c]			B3LYP/6-311++G(d,p)
No.	Species	Unscaled freq	Scaled freq.[a]	FT-IR	FT-Raman	Infrared gas	Infrared liquid	Raman liquid	TED[d] (⩾10%)
ν1	E''	26	26						φCH_3 (87) [τCCCH (87)]
ν2	E''	26	26						φCH_3 (96) [τCCCH (96)]
ν3	A''	28	28						φCH_3 (96) [τCCCH (96)]
ν4	A''	172	169			183	179 s	183 vs	γCH [τCCCC (57) + τCCCH (10)]
ν5	E''	221	217		231			231 vs	γCH [τCCCC (72) + τCCCH (10)]
ν6	E''	221	217						γCH [τCCCC (58) + τCCCH (18)]
ν7	E'	270	265						δCC—CH_3 (83)
ν8	E'	270	265		277	274	274 s	276 s	δCC—CH_3 (82)
ν9	A'	461	453					459 vw	δCC—CH_3 (90)
ν10	E'	522	513		517	519	516 w	515 vw	δCCC (50) + νCC (16) + δCC—CH_3 (10)
ν11	E'	522	513						δCCC (43) + νCC (14) + δCC—CH_3 (10)
ν12	E''	530	521						τCCCH (39) + τCCCC (20)
ν13	E''	530	521						τCCCC (32) + τCCCH (31)
ν14	A'	576	567		578	567	577 vw	578 vs	νC—CH_3 (48) + νCC (25)
ν15	A''	707	695	688		650, 678, 687, 694	648 vw, 687 s	652 vw, 688 vw	τCCCC (42) + τCCCH (33) [γCH]
							729 vw	719 vw	
							737 vw	730 vw	
							754 vw	750 vw	
ν16	A''	853	838	833		828, 836, 845	836 s	835 vw	γCH [τCCCH (70)]
ν17	E''	894	879	880			881 w	881 w	γCH [τCCCH (84)]
ν18	E''	894	879						γCH [τCCCH (88)]
ν19	E'	943	927	927		937, 929	929 w	930 w	νC—CH_3 (33) + νCC (18) + δCCH (12)) ring breathing
ν20	E'	943	927						νC—CH_3 (33) + νCC (22) + δCCC (11) + δCCH (10)) ring breathing
ν21	A'	1009	992		999			989 sh, 999 vs	νCC (31) + δCCC (29)
ν22	E'	1029	1012						ΓCH_3 [δCCH (40)] + νC—CH_3 (19) + νCC (11)
ν23	E'	1029	1012						ΓCH_3 [δCCH (45)] + νC—CH_3 (18) + νCC (10)
ν24	A'	1036	1018				1017 w		ΓCH_3 [δCCH (28)] + νCC (19)
ν25	E''	1059	1041	1038	1040		1038 s	1038 s	ΓCH_3 [δCCH (62)] + τCCCH (21)
ν26	E''	1059	1041						ΓCH_3 [δCCH (60)] + τCCCH (20)
ν27	A''	1060	1042			1042			ΓCH_3 [δCCH (59)] + τCCCH (19)
ν28	E'	1187	1167	1065	1070	1056	1166 w	1168 m	δCCH (53) + νC—CH_3 (18) + νCC (19)
ν29	E'	1187	1167					1218 vw	δCCH (53) + νC—CH_3 (18) + νCC (16)
ν30	A'	1296	1274						νCC (42) + νC—CH_3 (18) + δCCH (11)
ν31	A'	1321	1299		1302			1290 vw, 1301 vs	δCCH (57) + νC—CH_3 (17)
ν32	A'	1346	1323						νCC (48) + δCCH (27) + νC—CH_3 (10)
ν33	E'	1411	1387	1372	1382	1387, 1376	1376 m	1379 vs	φCH_3 [δCHH (51) + δCCH (44)]
ν34	E'	1411	1387						φCH_3 [δCHH (47) + δCCH (42)]
ν35	A'	1414	1390						φCH_3 [δCHH (50) + δCCH (42)]
ν36	E'	1457	1433				1418 w	1423 m	νCC (24) + δCHH (17) + τCCCH (12) + δCCH (10)
ν37	E'	1457	1433	1439			1443 w	1448 m	νCC (29) + δCHH (17) + δCCH (12) + τCCCH (10)
ν38	A''	1486	1460			1460			ΓCH_3 [δCHH (58)] + τCCCH (21)
ν39	E''	1487	1461						ΓCH_3 [δCHH (52)] + τCCCH (13) + δCCH (10)
ν40	E''	1487	1461						ΓCH_3 [δCHH (57)] + τCCCH (16)
ν41	A'	1496	1470	1470			1473 vs	1475 sh	φCH_3 [δCHH (56)] + δCCH (12)
ν42	E'	1513	1487						φCH_3 [δCHH (29)] + δCCH (19) + νCC (13)
ν43	E'	1513	1487			1490			φCH_3 [δCHH (34)] + δCCH (18) + νCC (10)
						1519, 1505	1511 vw		
ν44	E'	1641	1613				1563 vw, 1579 vw	1580 w	νCC (62)ring + δCCH (15)
ν45	E'	1641	1613	1608	1610	1615, 1609	1608 vs	1607 vs	νCC (64)ring + δCCH (15)
ν46	E'	3022	2895	2727	2750	2745 w	2730 m	2730 m	νCHsym. (96) [CH_3]
ν47	E'	3022	2895	2853	2890	2877 m	2860 s	2769 w	νCHsym. (95) [CH_3]
ν48	A'	3022	2895	2916			2918 s	2867 m	νCHsym. (100) [CH_3]
ν49	E''	3070	2941		2919	2932 s		2917 vs	νCHasym. (100) [CH_3]

Table 2 (*continued*)

Modes	Sym.	B3LYP/6-311++G(d,p)		Experimental[b]		Experimental[c]			B3LYP/6-311++G(d,p)
No.	Species	Unscaled freq	Scaled freq.[a]	FT-IR	FT-Raman	Infrared gas	Infrared liquid	Raman liquid	TED[d] (⩾10%)
ν50	E''	3070	2941	2946			2946 sh	2950 vw	νCHasym. (100) [CH_3]
ν51	A''	3070	2941						νCHasym. (100) [CH_3]
ν52	A'	3100	2969						νCHasym. (100) [CH_3]
ν53	E'	3100	2970				2970 sh		νCHasym. (97) [CH_3]
ν54	E'	3100	2970						νCHasym. (93) [CH_3]
ν55	E'	3145	3013	3007	3009			3006 s	νCHasym. (99) [Ring]
ν56	E'	3145	3013						νCHasym. (99) [Ring]
ν57	A'	3148	3016			3023 s	3017 s	3023 w	νCHsym. (99) [Ring]
								3210 vw	

ν; stretching, γ; out-of plane bending, δ; in-plane-bending, τ; torsion, ρ; scissoring, φ; twisting, Γ; rocking.
[a] Wavenumbers in the ranges from 4000 to 1700 cm^{-1} and lower than 1700 cm^{-1} are scaled with 0.958 and 0.983 for B3LYP/6-311++G(d,p) basis set, respectively.
[b] Taken from Ref. [22].
[c] The experimental datas of the study of mesitylene [9].
[d] TED: Total Energy Distribution.

pure modes. All results for the above conclusions are in well agreement for the literature of the similar molecule for C—H parameters [9,18,20,42,43].

CH_3 (Methyl group) modes

The mesitylene molecule has three methyl groups in the first, third and fifth position. For benzene derivatives containing a CH_3 group two bands which asymmetrical and symmetrical stretching occurs. The asymmetric stretching for the CH_3 and CH_2 groups as magnitude higher than the symmetric stretching. The CH stretching vibration of methyl groups appears at lower frequencies than those of aromatic ring (3000–3100 cm^{-1}). The asymmetric and symmetric stretching modes of methyl group attached the benzene ring are usually downshifted due to electronic effects and are expected near 2990, 2940 cm^{-1} asymmetric and 2860 cm^{-1} symmetric stretching vibrations. The asymmetric CH stretch vibrations of methyl group is expected around 2980 cm^{-1} and the symmetric one [47,48] occurs at ca. 2870 cm^{-1}. These modes (asymmetric and symmetric) were recorded at 3100--2900 cm^{-1}, the in-plane deformation around 1450–1370 cm^{-1} and the rocking around 1040–990 cm^{-1} [49]. In this work, observed wavenumbers were recorded at 2970, 2946 cm^{-1} (FT-IR) and at 2950, 2917 cm^{-1} (FT-Raman) for asymmetric and at 2918, 2860, 2730 cm^{-1} (FT-IR) and at 2867, 2769, 2730 cm^{-1} (FT-Raman) [9,22] symmetric and computed at 2970, 2895 cm^{-1} (B3LYP) and at 2934, 2865 cm^{-1} (HF) as a asymmetric and symmetric mode, respectively.

The title molecule mesitylene has three CH_3 groups at the substitution. The CH_3 stretching modes were discussed in the previous part. The rocking and twisting vibrations are also commented here. The methyl rocking mode usually appears within the region 1070–1010 cm^{-1} [50,51]. The intense infrared bands observed at 1373 cm^{-1} are among the CH_3 rocking [52]. The observed bands at 1045 and 1038 cm^{-1} are assigned to out-of-plane CH_3 rocking vibrations [53]. In the present investigation the modes CH_3 rocking were calculated at 1012 (double), 1018, 1041 (double), 1042, 1460 and 1461(double) cm^{-1} using B3LYP method, and also at 995, 1005 (double), 1049 (double), 1050, 1451 and 1452 (double) cm^{-1} with the HF method. These bands were observed at 1017, 1038 and 1460 cm^{-1} FT-IR and 1038 and 1040 cm^{-1} FT-Raman spectra [9].

The torsional modes appear in general in the low-wavenumber regions. Govindarajan et al. calculated normal modes involving the out of plane motion of CH_3 (torsion CH_3) start appearing below 250 cm^{-1} wavenumbers [53]. In the present work, these modes are assigned as torsional (twisting) modes and calculated below the 40 cm^{-1}. Other twisting (φCH_3) modes are computed at 1387 (double), 1390, 1470 and 1487 (double) cm^{-1} by using B3LYP method and at 1389 (double), 1395, 1458 and 1476 (double) cm^{-1} with the HF method. The observed data were presented at 1376, 1473 cm^{-1} (FT-IR) and at 1379, 1475 cm^{-1} (FT-Raman), respectively [9].

CC modes

The ring stretching vibrations are very much important and highly characteristic of the aromatic ring itself. The CC stretching vibrations modes in the phenyl ring are generally occur in the region 1430–1625 cm^{-1}. Varsanyi [54] observed at 1625–1590, 1575–1590, 1470–1540, 1430–1465 and 1280–1380 cm^{-1} from the frequency ranges given by for the five bands in the region and generally the bands are of variable intensity. The wavenumbers observed in the FT-IR spectrum at 1589 and 1516 cm^{-1} have been assigned to C=C stretching vibrations [55]. The C=C corresponding vibrations appear in FT-Raman spectrum at 1596 and 1541 cm^{-1} [55]. In this paper, the CC modes were computed at 513 (double), 567, 927–1018, 1167–1323, 1433 (double), 1487 (double) and 1613 (double) cm^{-1} by B3LYP method for mesitylene. The experimental values are in very good coherent observed data

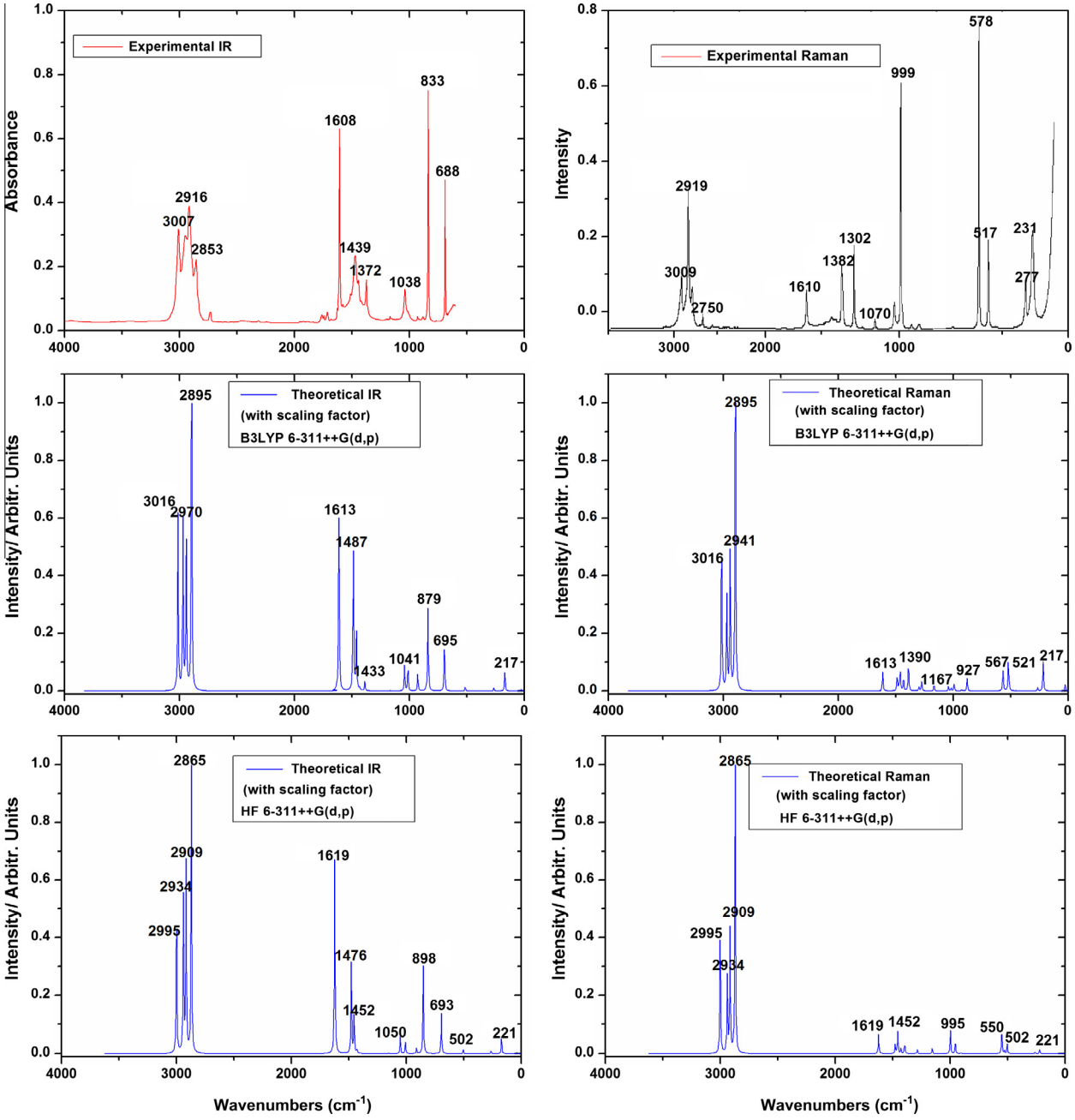

Fig. 2. The experimental and calculated infrared and Raman spectra of mesitylene.

as 516, 519, 567, 577, 929, 937, 1017, 1056, 1166, 1443, 1608, 1609, 1615 (FT-IR) [9] 927, 1065, 1439 and 1608 (FT-IR) [22] 515, 578, 930, 1168, 1448 and 1607 (FT-Raman) [9] 517, 578, 999, 1070 and 1610 (FT-Raman) [22]. The biggest contribution modes of CC stretching vibrations are calculated at 1613 (double) and 1619 (double) cm^{-1} with the TED contribution 64, 62 and 60, 62 percentages with B3LYP and HF method respectively, numbered modes no 44 and 45. As revealed by TED, the ring-breathing mode which can be described as the trigonal ring breathing vibration of the aromatic ring at 927 (double) with B3LYP and at 909 cm^{-1} (double) with HF, which was observed [9] at 929 and 930 cm^{-1} in infrared and Raman spectrum, respectively.

The ring modes in toluene [56] which contain one substituent attached to an aromatic ring are compared with mesitylene. Most of the ring modes of toluene are found to have significantly lower frequencies in mesitylene, which is trisubstituted in benzene. For example, the ring modes labeled 57, 55, 44, 37, 19 and 10 downshift, respectively, from 3079 cm^{-1}, 3072 cm^{-1}, 1587 cm^{-1}, 1445 cm^{-1}, 961 cm^{-1} and 522 cm^{-1} in toluene [56]. The frequency changes in the modes 44, 37, 19, and 10 are due to the changes in the force constant-reduced mass ratio resulting mainly from different extents of mixing between vibrations of the ring and substituent groups. The frequency reduction seen in the pure ring modes (57 and 55) with the inclusion of a substituent group to toluene can be explained based on the corresponding changes in the reduced masses and force constants.

The torsion and CCC bending modes are mixed with other modes. The calculated wavenumbers of these modes almost coincide with experimental data after scaling. The CCC bending modes (7–11) are assigned between ring and methyl group carbons.

C—CH_3 stretching modes

The C—CH_3 vibrations are important modes for the molecules had methyl groups. These modes are generally contaminated with C—H in-plane bending vibration [57]. The active fundamental mode identified as C—CH_3 was observed at 1214 cm^{-1} in FT-IR and at 1217 cm^{-1} in FT-Raman [58]. The C—CH_3 stretching mode shows good agreement with computed wavenumber at 567, 927 (double), 1012 (double) 1167 (double), 1274, 1299 and 1323 cm^{-1} using B3LYP method. The most contributions of C—CH_3 stretching vibrations are showed 567 cm^{-1} modes number 14. This mode (ν14) is observed at 567, 577 cm^{-1} in FT-IR [9] 578 cm^{-1} FT-Raman [9,22]. These modes also showed parallel the calculations of HF method. Our results are best agreement the literature [57].

NMR calculations

Nuclear magnetic resonance is a research technique that exploits the magnetic properties of certain atomic nuclei to determine physical and chemical properties of atoms or the molecules in which they are contained. It relies on the phenomenon of nuclear magnetic resonance and can provide detailed information about the structure, dynamics, reaction state, and chemical environment of molecules. NMR most frequently is used by researchers to investigate the properties of organic molecules, though it is applicable to any kind of sample that contains nuclei possessing spin. We also have been studied NMR calculations, because of the accurate predictions of molecular geometries are essential for reliable calculations of magnetic properties.

In this paper, ^1H and ^{13}C chemical shifts of the title molecule in chloroform solution solvent are gathered in Table 3. The atom statues were numbered according to Fig. 1. The experimental ^1H and ^{13}C NMR spectra of the mesitylene are given in Fig. S1a and b, respectively. In the first instance, the full geometry optimization of the studied molecule was performed at the gradient corrected density functional level of theory using the hybrid B3LYP method based on Becke's three parameters functional of DFT and gauge-including atomic orbital (GIAO) [32,33]. ^1H and ^{13}C chemical shift calculations of the compound was made by the same method using 6-311++G(d,p) basis set in chloroform solution. The isotropic shielding values were used to calculate the isotropic chemical shifts δ with respect to tetramethylsilane (TMS).

The proton chemical shift (^1H NMR) of organic molecules generally varies greatly with the electronic environment of the proton. Hydrogen attached or nearby electron- withdrawing atom or group can decrease the shielding and move the resonance of attached proton towards to a higher frequency, whereas electron-donating atom or group increases the shielding and moves the resonance towards to a lower frequency [59]. The chemical shifts of aromatic protons of organic molecules are usually observed in the range of 7.00–8.00 ppm. The signals of the 3 aromatic protons (^1H) of the title compound were calculated theoretically 6.89–7.00 and 6.99–7.09 ppm, for gas and chloroform solvent, respectively, reported at 6.78 ppm as showed triplet experimentally in chloroform solvent. The chemical shift value of H_7, H_8 and H_9 attached the carbon atoms of the phenyl ring is larger than the methyl proton signals due to the electron withdrawing properties of attached groups and high symmetry of the molecule. On the other hand the methyl protons lower than protons of the ring this can be due to the electronic charge density around of the ring. The protons resonance in this region could not be assigned unambiguously one by one due to overlap experimentally.

Aromatic carbons give signals in overlapped areas of the spectrum with chemical shift values from 100 to 150 ppm [60,61]. The molecule has nine carbons however these carbons three different groups as in the ring (attached H atoms and CH_3) and methyl carbons, which is consistent with the structure on basis of molecular symmetry. If we consider ^{13}C NMR the chemical shifts of the title molecule there are three symmetric groups (C_1, C_3 and C_5), (C_2, C_4 and C_6) and (C_{10}, C_{14} and C_{18}) are observed 137.66, 126.99 and 21.17 respectively, calculated nearly same correlations and slightly larger than experimental data. The C_1, C_3 and C_5 carbons, attached the methyl groups, is larger than the other carbons of the ring at about 10 ppm. This increment can be due to the CH_3 groups. Namely, these groups that electronegative substituent polarizes the electron distribution in its bond to carbon. The chemical shifts value of C_1, C_3 and C_5 bonded to methyl was observed 137.66 ppm, which was calculated ca. 144 ppm. The other ^{13}C NMR chemical shifts in the ring for the title molecule C_2, C_4 and C_6 were recorded 126.99 ppm and predicted ca. 130 ppm. ^{13}C NMR chemical shift of C_{10}, C_{14} and C_{18} atoms is smaller than the other ring carbon atoms.

Both experimentally and theoretically chemical shifts are showing good correlation with each other (Table 3). The correlation graphics between the experimental and calculated ^{13}C NMR and ^1H NMR chemical shifts of title molecule are represented in Fig. 3. The relations between the calculated and experimental wavenumbers chemical shifts (δ_{exp}) are usually linear and described by the following equation:

$$\delta_{cal}(ppm) = 1.0388\delta_{exp} - 0.1204 \quad R^2 = 0.9999$$

In present study, the following linear relationships were obtained for ^{13}C and ^1H chemical shifts.

Table 3
Experimental and theoretical, ^1H and ^{13}C NMR isotropic chemical shifts (with respect to TMS) of mesitylene with DFT (B3LYP 6-311++G(d,p)) method.

Atoms	Exp.[a]	Gas	CDCl3	Atoms	Exp.[a]	Gas	CDCl3
C(1)	137.66	144.02	144.69	H(7)	6.78	7.00	7.09
C(2)	126.99	130.90	130.56	H(8)	6.78	6.95	7.04
C(3)	137.66	143.85	144.50	H(9)	6.78	6.89	6.99
C(4)	126.99	130.37	130.14	H(11)	2.26	2.48	2.52
C(5)	137.66	143.79	144.48	H(12)	2.26	2.48	2.52
C(6)	126.99	130.83	130.56	H(13)	2.26	1.79	1.86
C(10)	21.17	22.06	21.75	H(15)	2.26	2.42	2.46
C(14)	21.17	21.90	21.58	H(16)	2.26	1.81	1.88
C(18)	21.17	21.90	21.58	H(17)	2.26	2.42	2.46
				H(19)	2.26	2.42	2.46
				H(20)	2.26	1.77	1.84
				H(21)	2.26	2.42	2.46

[a] Taken from Ref. [23].

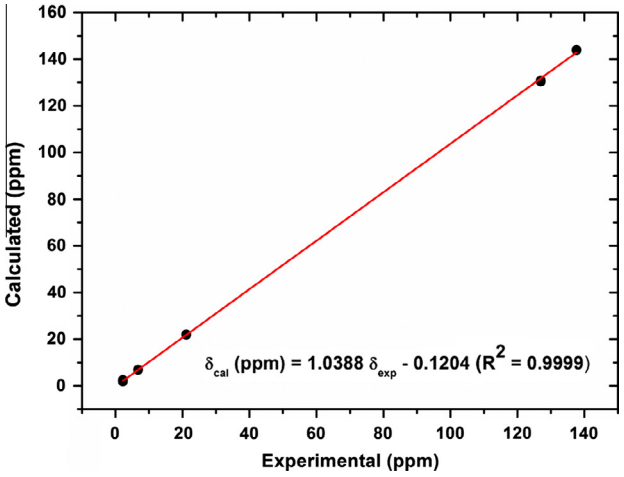

Fig. 3. The correlation graphics of calculated and experimental chemical shifts of mesitylene.

$$^{13}C : \delta_{cal}(ppm) = 1.039\delta_{exp} - 0.1455 \quad R^2 = 0.9997$$

$$^{1}H : \delta_{cal}(ppm) = 1.0445\delta_{exp} - 0.1350 \quad R^2 = 0.9821$$

The performances of the B3LYP method 6-311++G(d,p) basis set with respect to the prediction of the relative shielding within the molecule were nearly close. However, ^{13}C NMR calculations gave a slightly better coefficient and lower standard error (R^2 = 0.9997) than for ^{1}H (R^2 = 0.9821) chemical shifts. Also the correlation graphs of the ^{1}H and ^{13}C NMR are given Figs. S2 and S3.

Electronic properties

UV spectra

To investigate UV spectrum analyses of the mesitylene were researched by theoretical calculation with combined experimental results [22]. The electronic absorption spectra of title molecule had been measured in ethanol at room temperature. To obtain some electronic properties such as; the excitation energies, absorbance and oscillator strengths for the title molecule, we were optimized geometry of the molecule in the ground state by using TD-DFT calculations with the B3LYP/6-311++G(d,p) method in some organic solvents. The TD-DFT method predicts the electronic absorption spectra of the mesitylene as a quite reasonable method. The experimental absorption wavelengths (energies) and computed electronic values, such as absorption wavelength (λ), excitation energies (E), oscillator strengths (f), and major contributions of the transitions and assignments of electronic transitions are tabulated in Table 4. The strong π–π^* and σ–σ^* transition of the molecule are emerge from in the UV–Vis region with high extinction coefficients [62]. Experimentally recorded maximum absorption values are 211.05 and 265.00 nm owing to π–π^* transition in ethanol [22]. The absorption values are computed at 218.68 and 243.05 nm in also ethanol solvent.

Frontier molecular orbital analysis

The FMOs, called highest occupied molecular orbital (HOMO) and lowest unoccupied molecular orbital (LUMO) are generally more important than the others of them. These orbitals play a significant role to determine the way the molecule interacts with other species. Also the energy is very useful for physicists and chemists and the main orbital taking part in chemical reaction. The HOMO energy characterizes the ability of electron giving; LUMO characterizes the ability of electron accepting. While the energy of the HOMO is directly related to the ionization potential, LUMO energy is directly related to the electron affinity. This electronic absorption corresponds to the transition from the ground to the first excited state and is mainly described by one electron excitation from the highest occupied molecular orbital to the lowest unoccupied molecular orbital. [63,64].

We want to understand the bonding scheme of the mesitylene and pictured the surfaces of FMOs as a Fig. 4. The HOMO and LUMO energy calculated by B3LYP/6-311++G(d,p) method. The energy gap between HOMO and LUMO orbital which is a critical parameter in determining molecular electrical transport properties because it is a measure of electron conductivity, were calculated 6.22 eV for title molecule. The knots of HOMO and LUMO are placed nearly similarly in terms of location on the ring or methyl groups. However there are four nodes of the HOMO on the ring and two nodes on methyl for two of three groups. However, the nodes of LUMO located as two nodes on ring. Also on the methyl groups the nodes changed but the same image are seen. The red and green colors are positive and negative phase, respectively. Moreover, energy gap of the title molecule are presented in Fig. 4. The percentages of the transition of the molecule are given in Table 4 only major contributions. The most contribution were predicted at 218.68 nm as a π–π^* transition percentage 67 (H − 1 → L + 2). However the H → L and H − 1 → L + 1 transition are computed the same percentage (34%) at the 243.05 nm highest transition.

Total, partial, and overlap population density-of-states

The DOS (or TDOS) plot is to presentation of molecule orbital (MO) compositions and their contributions to chemical bonding through the OPDOS (or COOP) plot. The bonding, anti-bonding and nonbonding natures of the interaction of the two orbitals, atoms or groups explain the OPDOS (or COOP) diagrams. The value can be positive, negative or zero, the OPDOS it indicates a bonding interaction (because of the positive overlap population), an anti-bonding interaction (due to negative overlap population) and non-bonding interactions, respectively [65]. Additionally, the OPDOS diagrams allow us to the determination and comparison of the donor–acceptor properties of the ligands and ascertain the bonding, non-bonding. In the boundary region, neighboring orbitals may show quasi degenerate energy levels. In such cases, consideration of only the HOMO and LUMO may not yield a realistic description of the frontier orbitals [66–68].

To provide a pictorial representation of MO compositions and their contributions to chemical bonding, The TDOS, PDOS and OPDOS density of states of the mesitylene are plotted in Figs. 5–7, respectively, created by convoluting the molecular orbital information with Gaussian curves of unit height and Full width at half maximum (FWHM) of 0.3 eV using the GaussSum 2.2 program [38]. If one sees these Figs. 5–7 can conclude HOMO and LUMO energy construction and groups energy distribution (benzene and methyl) and also defined the bonding character of the title molecule according to TDOS, PDOS and OPDOS figures respectively. As also seen Fig. 4 HOMO orbitals are localized on the ring and three CH_3 (methyl) groups their contributions about 92 and 8% respectively. Similarly, the LUMO orbitals are localized on the ring (83%) and two CH_3 groups (17%) of the compound. However the OPDOS diagram is shown Fig. 7 and some of orbitals of energy values of interaction between selected groups which are shown from figures easily, Phenyl ring ↔ CH_3 groups (blue line) system is negative (bonding interaction).

Molecular electrostatic potential surface

In order to understand the molecular electrostatic potential surface (MEPs) of mesitylene molecule in 3D plots is mapped and given in Fig. 8 by using checkpoint file of the output file of the DFT/B3LYP method 6-311++G(d,p) basis set due to having the most stable energy for the molecule. The molecular electrostatic potential

Table 4
Experimental and calculated absorption wavelengths λ (nm), excitation energies (eV), oscillator strengths (f) in ethanol solution.

Experimental		Calculated TD-DFT/B3LYP/6-311++G(d,p)			
λ (nm)	E (eV)	λ (nm)	E (eV)	Assignments	Major contributes [a]
265.00	4.6566	243.05	5.1019	π–π^*	H → L (34%), H-1 → L + 1 (34%), H → L + 1 (15%), H-1 → L (15%)
211.05	5.8470	218.68	5.6705	π–π^*	H-1 → L + 2 (67%), H → L + 2 (31%)

[a] H: HOMO, L: LUMO.

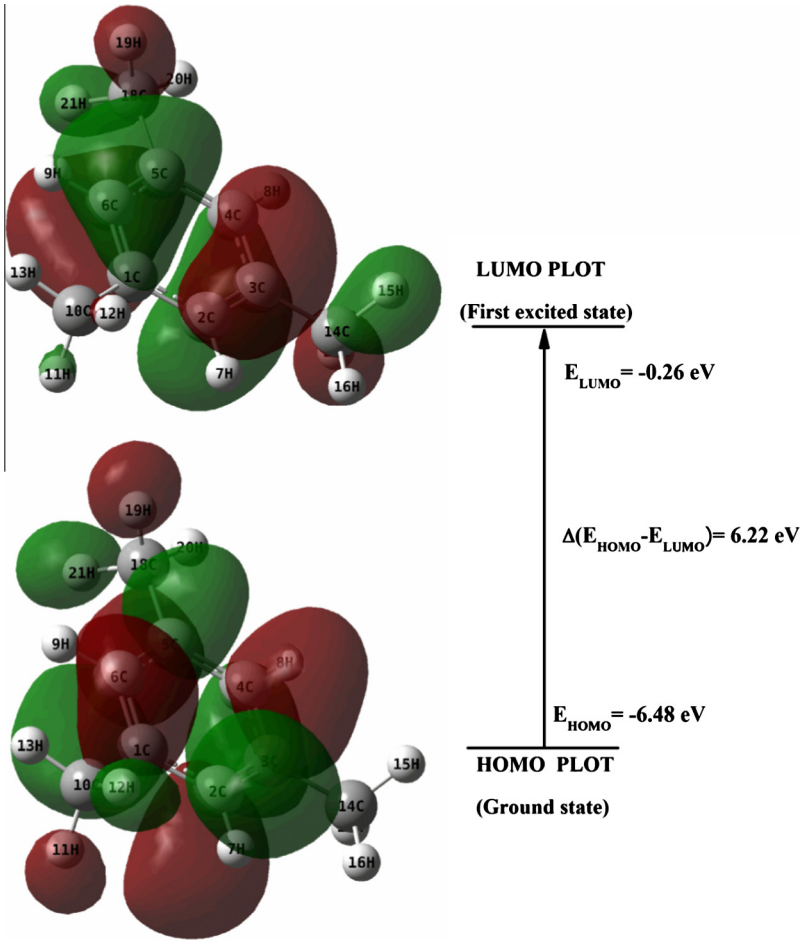

Fig. 4. The frontier molecular orbitals of mesitylene.

surface (MEPs) is a plot of electrostatic potential mapped onto the constant electron density surface. The MEPs superimposed on top of the total energy density as a shell. Because of the usefulness feature to study reactivity given that an approaching electrophile will be attracted to negative regions (where the electron distribution effect is dominant). In the majority of the MEPs, while the maximum negative region which preferred site for electrophilic attack indications as red color, the maximum positive region which preferred site for nucleophilic attack symptoms as blue color. The importance of MEPs lies in the fact that it simultaneously displays molecular size, shape as well as positive, negative and neutral electrostatic potential regions in terms of color grading and is very useful in research of molecular structure with its physicochemical property relationship [69,70].

According to the MEPs of mesitylene molecule in 3D plots (Fig. 8), the different values of the electrostatic potential at the

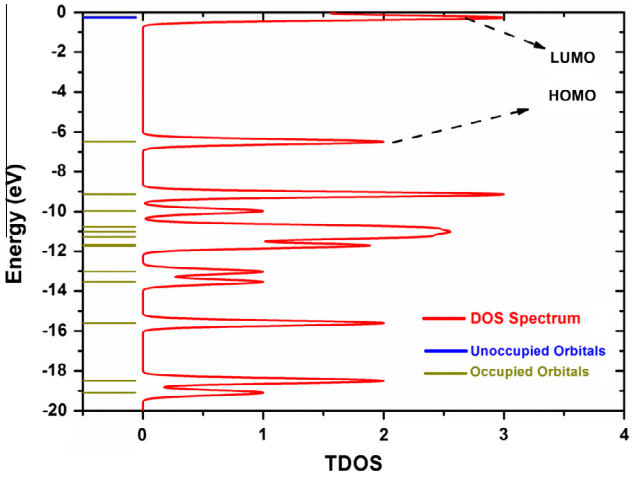

Fig. 5. The calculated TDOS diagrams for mesitylene.

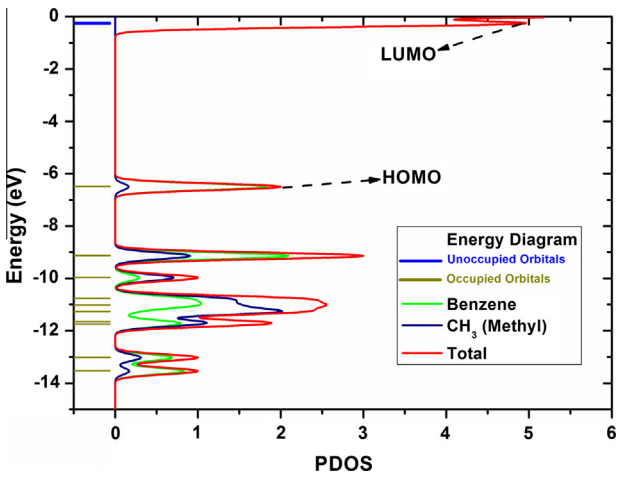

Fig. 6. The calculated PDOS diagrams for mesitylene.

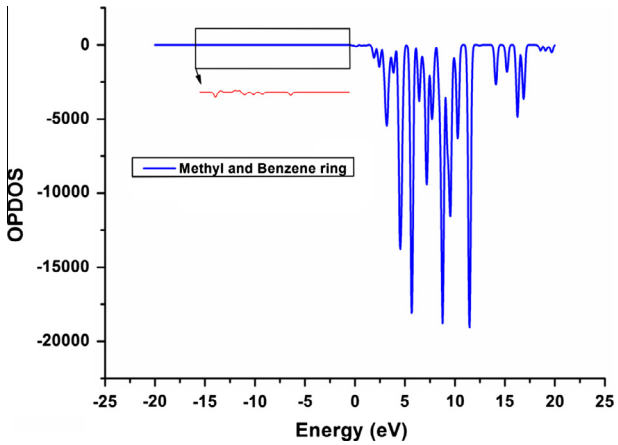

Fig. 7. The OPDOS (or COOP) diagrams for mesitylene.

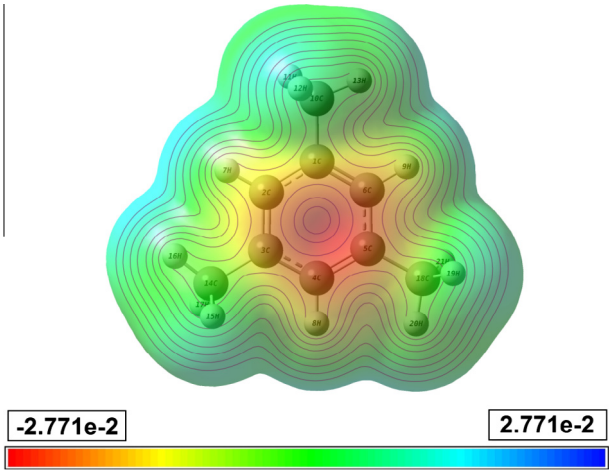

Fig. 8. Molecular electrostatic potential map of mesitylene.

surface are represented by different colors in the map of MEPs. The potential increases in the order from red to blue color. The color code of the maps is in the range between −0.02771 a.u. (dark red) and 0.02771 a.u. (dark blue) in compound, where blue indicates the strongest attraction and red indicates the strongest repulsion. As can be seen from the MEPs map of the title molecule, while there is no region having the positive potential, there is the negative potential middle of the ring of the title molecule. As a result, the molecule has no strongest attraction but, has the strongest repulsion (see Fig. 8).

Mulliken atomic charges

The atomic charges are an important for the application of quantum mechanical calculations of the molecular system. The Mulliken atomic charges of the mesitylene, toluene m-xylene and benzene are computed by the DFT/B3LYP method 6-311++G(d,p) basis set. We chose benzene and these three molecules according to number of CH_3 (methyl) groups attached the benzene ring. The Mulliken atomic charges of from benzene to mesitylene are given in Table 5. The results show that substitution of the aromatic ring leads to a redistribution of electron density. To show this effect of methyl groups the result of atomic charges are given and evaluated.

The carbon atoms attached the methyl are showed different charges according to evaluations of number of methyl group. Also the carbons near the methyl group or groups are tending to same

Table 5
Mulliken charges of from benzene to mesitylene [B3LYP/6-311++G(d,p)].

Benzene		Toluene		m-xylene		Mesitylene	
Atoms	Charges	Atoms	Charges	Atoms	Charges	Atoms	Charges
C1	−0.156	C1	0.663	C1	1.828	C1	1.533
C2	−0.155	C2	−0.328	C2	−2.149	C2	−1.685
C3	−0.155	C3	−0.273	C3	1.828	C3	1.533
C4	−0.156	C4	−0.100	C4	−1.097	C4	−1.685
C5	−0.155	C5	−0.273	C5	0.262	C5	1.533
C6	−0.155	C6	−0.328	C6	−1.097	C6	−1.685
H7	0.155	H7	0.144	H7	0.064	C10	−0.408
H8	0.155	H8	0.144	H8	0.098	C14	−0.408
H9	0.155	H9	0.144	H9	0.098	C18	−0.408
H10	0.155	H10	0.155	H10	0.155	H7	0.090
H11	0.155	H11	0.155	C11	−0.345	H8	0.090
H12	0.155	C12	−0.539	H12	0.108	H9	0.090
		H13	0.158	H13	0.108	H11	0.162
		H14	0.139	H14	0.134	H12	0.162
		H15	0.139	C15	−0.345	H13	0.145
				H16	0.108	H15	0.162
				H17	0.134	H16	0.145
				H18	0.108	H17	0.162
						H19	0.162
						H20	0.145
						H21	0.162

charges. The charges of hydrogen atoms methyl groups are nearly close magnitude all CH_3 in the molecules. However the results show that substitution of the phenyl ring by CH_3 groups lead to a redistribution of electron density symmetrically. Namely, the charge of molecule show symmetric distribution (negative or positive) due to the symmetry of CH_3 groups for the molecule. The all carbons of benzene are showed negative charges. But when the methyl group attached the carbon atom, the carbon charges are changed from negative to positive. As a result the carbon atoms showed different charges due to the CH_3 groups.

Thermodynamic properties

The thermodynamic parameters supply helpful and extra information about the title molecule. Therefore, some values (such as zero-point vibrational energy, thermal energy, specific heat capacity, rotational constants, entropy and dipole moment) of the studied molecule by DFT/B3LYP/6-311++G(d,p) method at 298.15 K in ground state are listed in the Table S1. The global minimum energy obtained for structure optimization of B3LYP with 6-311++G(d,p) basis set is −350.29372209 Hartree. At the same time, we investigated and listed in Table 6 the statically thermodynamic functions: heat capacity (C), entropy (S) and enthalpy changes (H) for the title

Table 6
Thermodynamic properties at different temperatures at the B3LYP/6-311++G(d,p) level for mesitylene.

T (K)	C (cal mol^{-1} K^{-1})	S (cal mol^{-1} K^{-1})	H (kcal mol^{-1} K^{-1})
100	16.575	72.004	1.421
150	20.944	80.355	2.458
200	25.506	87.569	3.717
250	30.463	94.229	5.214
298.15	35.561	100.386	6.898
300	35.761	100.610	6.968
350	41.175	106.836	8.991
400	46.473	112.947	11.282
450	51.494	118.948	13.832
500	56.159	124.828	16.624
550	60.448	130.574	19.641
600	64.376	136.177	22.862
650	67.972	141.633	26.271
700	71.268	146.940	29.853

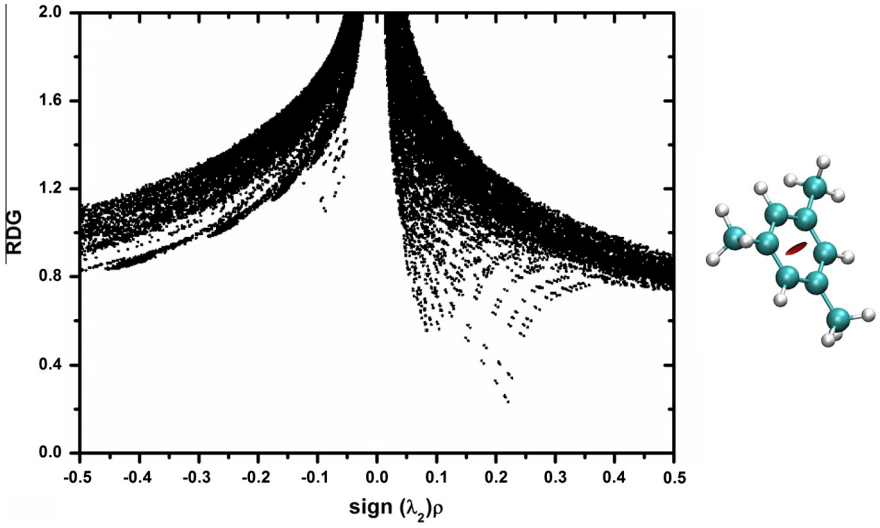

Fig. 9. Reduced density gradient for mesitylene.

molecule, obtained from the theoretical harmonic frequencies. As seen from the Table 6, it can be observed that these thermodynamic functions are increasing with temperature ranging from 100 to 700 K, varied every 50 K due to the fact that the molecular vibrational intensities increase with temperature. The correlation equations between heat capacity, entropy, enthalpy changes and temperatures were fitted by quadratic formulas and the corresponding fitting factors (R^2) for these thermodynamic properties are 0.9985, 0.9998 and 0.9999, respectively. The corresponding fitting equations are as follows and the correlation graphics of those shown in Fig. S4.

$$C = 4.7250 + 0.1157T - 2.6380 \times 10^{-5}T^2 \quad (R^2 = 0.9985)$$

$$S = 57.8622 + 0.1534T - 3.8004 \times 10^{-5}T^2 \quad (R^2 = 0.9998)$$

$$H = 0.0050 + 0.0088T - 4.8534 \times 10^{-5}T^2 \quad (R^2 = 0.9999)$$

Also one can be used to compute the other thermodynamic energies according to relationships of thermodynamic functions and estimate directions of chemical reactions according to the second law of thermodynamics in Thermochemical field. Notice: all thermodynamic calculations were done in gas phase and they could not be used in solution.

Reduced density gradient (RDG)

In order to investigate the weak interactions in real space based on the electron density and its derivatives were developed an approach by Johnson et al. [71]. The RDG is a fundamental dimensionless quantity coming from the density and its first derivative:

$$\mathrm{RDG}(r) = \frac{1}{2(3\pi^2)^{1/3}} \frac{|\nabla\rho(r)|}{\rho(r)^{4/3}}$$

RDG density tails show that; large, negative values of sign(λ_2)ρ are indicative of attractive interactions (such as dipole–dipole or hydrogen bonding); while if sign(λ_2)ρ is large and positive, the interaction is nonbonding. Values near zero indicate very weak, van der Waals interactions. The sign of λ_2 is utilized to distinguish the bonded ($\lambda_2 < 0$) from non-bonded ($\lambda_2 > 0$) interactions. [71]. The RDG of mesitylene were graphed by Multiwfn and plotted by VMD program [35,39] and this representation is given in Fig. 9. According to this representation of the RDG showed non-bonded ($\lambda_2 > 0$) interactions and red indicates strong non-bonded overlap. The molecule had the symmetrical structure both electron density and the bonding character. The region interaction marked by red can be identified as steric affect.

Conclusion

The detailed interpretations of the molecular structure, vibrational spectra, electronic and Mulliken charge analysis; thermodynamical properties and RDG of mesitylene were presented in this paper. The geometrical parameters of mesitylene were computed by DFT and HF calculations with a good accuracy when compared with experimental analysis of structurally very similar compound. The correlations of the statistical thermodynamics according to temperature are also presented. All results which were examined before by the experimental (IR, Raman, NMR and UV spectra) were supported by the computed results, comparing with experimental characterization data; vibrational wavenumbers, absorption wavelengths, electronic properties and chemical shifts values are in fairly good agreement with the experimental results. The predicted calculations are compared with experimental and showed an acceptable general agreement.

Appendix A. Supplementary material

Supplementary data associated with this article can be found, in the online version, at http://dx.doi.org/10.1016/j.saa.2013.07.070.

References

[1] M. Utsuro, M. Sugimoto, J. Nucl. Sci. Technol. 14 (5) (1977) 390–392.
[2] K.S. Pitzer, D.W. Scott, J. Am. Chem. Soc. 65 (1943) 803–829.
[3] V. Santhamma, Curr. Sci. 23 (1954) 118–119.
[4] M.A. Kovner, Opt. Spelctroskopiya. 1 (1956) 348–363.
[5] J.H.S. Green, W. Kynaston, H.A. Gebbie, Spectrochim. Acta A 19 (1963) 807–810.
[6] J.H.S. Green, D.J. Harrison, Spectrochim. Acta A 26 (1970) 1925–1937.
[7] J.H.S. Green, D.J. Harrison, W. Kynaston, Spectrochim. Acta A 27 (1971) 793–806.
[8] C.L. Lau, R.G. Snyder, Spectrochim. Acta A 27 (1971) 2073–2088.
[9] B.V. Lokshin, V.T. Aleksanyan, M.G. Ezernitskaya, Russian Chem. Bull. 31 (10) (1982) 1995–1999.
[10] L. Cser, K. Holderna-Natkaniec, I. Natkaniec, A. Pawlukojc, Physica B 276 (2000) 296–297.
[11] E.L. Hommel, H.C. Allen, Analyst 128 (2003) 750–755.
[12] H.I. Lee, M.S. Kim, J. Raman Spectrosc. 17 (1986) 269–272.
[13] M. Prager, H. Grimm, I. Natkaniec, Phys. Chem. Chem. Phys. 7 (2005) 2587–2593.
[14] E. Ferguson, J. Chem. Phys. 21 (1953) 886–990.

[15] M. Plazanet, M.R. Johnson, A. Cousson, J. Meinnel, H.P. Trommsdorff, Chem. Phys. 285 (2002) 299–308.
[16] R. Świercz, W. Wąsowicz, W. Majcherek, Polish J. Environ. Stud. 15 (3) (2006) 485–492.
[17] C.J. Egan, W.C. Buss, J. Phys. Chem. 63 (11) (1959) 1887–1890.
[18] J. Meinnel, A. Boudjada, A. Boucekkine, F. Boudjada, A. Moreac, S.F. Parker, J. Phys. Chem. A 112 (2008) 11124–11141.
[19] G. Davidson, E.M. Riley, J. Organometal. Chem. 19 (1969) 101–114.
[20] O. Hernandez, K.S. Knight, W. Van Beek, A. Boucekkine, A. Boudjada, W. Paulus, J. Meinnel, J. Mol. Struct. 791 (2006) 41–52.
[21] G. Fogarasi, P. Pulay, in: J.R. Durig (Ed.), Vibrational Spectra and Structure, vol. 14, Elsevier, Amsterdam, 1985.
[22] P.J. Linstrom, W.G. Mallard (Eds.), NIST Chemistry Web Book, NIST Standard Reference Database Number 69, National Institute of Standards and Technology, Gaithersburg MD, 20899, http://webbook.nist.gov, (retrieved September 6, 2013) (NIST Chemistry Web book, IR database. http://srdata.nist.gov/cccbdb).
[23] SDBS Web: http://sdbs.riodb.aist.go.jp (National Institute of Advanced Industrial Science and Technology, retrieved September 6, 2013).
[24] P. Hohenberg, W. Kohn, Phys. Rev. 136 (1964) B864–B871.
[25] A.D. Becke, J. Chem. Phys. 98 (1993) 5648–5652.
[26] C. Lee, W. Yang, R.G. Parr, Phys. Rev. B 37 (1988) 785–789.
[27] M.J. Frisch et al., GAUSSIAN 09, Revision A.1, Gaussian, Inc., Wallingford, CT, 2009.
[28] D.C. Young, Computational Chemistry: A Practical Guide for Applying Techniques to Real World Problems (Electronic), John Wiley & Sons Inc., New York, 2001.
[29] N. Sundaraganesan, S. Ilakiamani, H. Salem, P.M. Wojciechowski, D. Michalska, Spectrochim. Acta A 61 (2005) 2995–3001.
[30] J. Baker, A.A. Jarzecki, P. Pulay, J. Phys. Chem. A 102 (1998) 1412–1424.
[31] SQM version 1.0, Scaled Quantum Mechanical Force Field, 2013 Green Acres Road, Fayetteville, Arkansas 72703.
[32] R. Ditchfield, J. Chem. Phys. 56 (1972) 5688–5691.
[33] K. Wolinski, J.F. Hinton, P. Pulay, J. Am. Chem. Soc. 112 (1990) 8251–8260.
[34] M. Petersilka, U.J. Gossmann, E.K.U. Gross, Phys. Rev. Lett. 76 (1966) 1212–1215.
[35] E. Runge, E.K.U. Gross, Phys. Rev. Lett. 52 (1984) 997–1000.
[36] R. Bauernschmitt, R. Ahlrichs, Chem. Phys. Lett. 256 (1996) 454–464.
[37] C. Jamorski, M.E. Casida, D.R. Salahub, J. Chem. Phys. 104 (1996) 5134–5147.
[38] N.M. O'Boyle, A.L. Tenderholt, K.M. Langner, J. Comp. Chem. 29 (2008) 839–845.
[39] W. Humphrey, A. Dalke, K. Schulten, J. Mol. Graph. 14 (1996) 33–38.
[40] M. Govindarajan, M. Karabacak, Spectrochim. Acta A 96 (2012) 421–435.
[41] M. Govindarajan, M. Karabacak, Spectrochim. Acta A 94 (2012) 36–47.
[42] M. Karabacak, D. Karagöz, M. Kurt, J. Mol. Struct. 892 (2008) 25–31.
[43] M. Govindarajan, K. Ganasan, S. Periandy, M. Karabacak, S. Mohan, Spectrochim. Acta A 77 (2010) 1005–1013.
[44] N.B. Colthup, L.H. Daly, S.E. Wiberley, Introduction to Infrared and Raman Spectroscopy, Academic Press, New York, 1964.
[45] M. Silverstein, G.C. Basseler, C. Morill, Spectrometric Identification of Organic Compounds, Wiley, New York, 2001.
[46] V. Arjunan, I. Saravanan, P. Ravindran, S. Mohan, Spectrochim. Acta A 74 (2009) 375–384.
[47] D. Sajan, I. Hubert Joe, V.S. Jayakumar, J. Raman Spectrosc. 37 (2005) 508–519.
[48] M. Gussoni, C. Castiglioni, M.N. Ramos, M.C. Rui, G. Zerbi, J. Mol. Struct. 224 (1990) 445–470.
[49] J.F. Arenas, I. Tocon, J.C. Otero, J.I. Marcos, J. Mol. Struct. 410–411 (1997) 443–446.
[50] A. Altun, K. Golcuk, M. Kumru, J. Mol. Struct. (Theochem) 637 (2003) 155–169.
[51] H. Endredi, F. Billes, G. Keresztury, J. Mol. Struct. (Theochem) 677 (2004) 211–225.
[52] H.M. Badawi, Spectrochim. Acta A 87 (2012) 11–14.
[53] M. Govindarajan, M. Karabacak, Spectrochim. Acta A 110 (2013) 314–324.
[54] G. Varsanyi, Assignments of Vibrational Spectra of Seven Hundred Benzene Derivatives, vol. 1–2, Springer, 1974.
[55] M.K. Rofouei, N. Sohrabi, M. Shamsipur, E. Fereyduni, S. Ayyappan, N. Sundaraganesan, Spectrochim. Acta A 76 (2010) 182–190.
[56] H.F. Hameka, J.O. Jensen, J. Mol. Struct. (Theochem) 362 (1996) 325.
[57] V. Krishnakumar, S. Dheivamalar, Spectrochim. Acta A 71 (2008) 465–470.
[58] M. Karabacak, E. Yilan, Spectrochim. Acta A 87 (2012) 273–285.
[59] N. Subramania, N. Sundaraganesan, J. Jayabharathi, Spectrochim. Acta A 76 (2010) 259–269.
[60] H.O. Kalinowski, S. Berger, S. Braun, Carbon-13 NMR Spectroscopy, John Wiley & Sons, Chichester, 1988.
[61] K. Pihlajar, E. Kleinpeter (Eds.), Carbon-13 Chemical Shifts in Structural and Sterochemical Analysis, VCH Publishers, Deerfield Beach, 1994.
[62] F.A. Cotton, C.W. Wilkinson, Advanced Inorganic Chemistry, third ed., Interscience Publisher, New York, 1972.
[63] K. Fukui, Science 218 (1982) 747–754.
[64] S. Gunasekaran, R.A. Balaji, S. Kumaresan, G. Anand, S. Srinivasan, Can. J. Anal. Sci. Spectrosc. 53 (2008) 149–160.
[65] M. Chen, U.V. Waghmare, C.M. Friend, E. Kaxiras, J. Chem. Phys. 109 (1998) 6854–6860.
[66] R. Hoffmann, Solids and Surfaces: A Chemist's View of Bonding in Extended Structures, VCH Publishers, New York, 1988.
[67] T. Hughbanks, R. Hoffmann, J. Am. Chem. Soc. 105 (1983) 3528–3537.
[68] J.G. Małecki, Polyhedron 29 (2010) 1973–1979.
[69] J.S. Murray, K. Sen, Molecular Electrostatic Potentials, Concepts and Applications, Elsevier, Amsterdam, 1996.
[70] E. Scrocco, J. Tomasi, in: P. Lowdin (Ed.), Advances in Quantum Chemistry, Academic Press, New York, 1978.
[71] E.R. Johnson, S. Keinan, P. Mori-Sánchez, J. Contreras-García, A.J. Cohen, W. Yang, J. Am. Chem. Soc. 132 (2010) 6498–6506.